HHS Public Access

Author manuscript

Biochemistry. Author manuscript; available in PMC 2024 July 18.

Published in final edited form as:

Biochemistry. 2023 July 18; 62(14): 2216–2227. doi:10.1021/acs.biochem.3c00227.

Targeting the conformational change in ArnA dehydrogenase for selective inhibition of polymyxin resistance

Megan E. Mitchell[1], **Petia Z. Gatzeva-Topalova**[1,#], **Austin D. Bargmann**[2], **Tarek Sammakia**[2,†], **Marcelo C. Sousa**[1,*]

[1]Department of Biochemistry, University of Colorado Boulder, Boulder, CO 80309;

[2]Department of Chemistry, University of Colorado Boulder, Boulder, CO 80309

Abstract

Polymyxins are important last resort antibiotics for the treatment of infections caused by multidrug resistant Gram-negative pathogens. However, pathogens have acquired resistance to polymyxins through a pathway that modifies lipid A with 4-amino-4-deoxy-L-arabinose (Ara4N). Inhibition of this pathway is, therefore, a desirable strategy to combat polymyxin resistance. The first pathway-specific reaction is an NAD^+-dependent oxidative decarboxylation of UDP-glucuronic acid (UDP-GlcA) catalyzed by the dehydrogenase domain of ArnA (ArnA_DH). We present the crystal structure of *Salmonella enterica* serovar Typhimurium ArnA in complex with UDP-GlcA showing that binding of the sugar nucleotide is sufficient to trigger a conformational change conserved in bacterial ArnA_DHs but absent in its human homologs, as confirmed by structure and sequence analysis. Ligand binding assays show that the conformational change is essential for NAD^+ binding and catalysis. Enzyme activity and binding assays show that: (i) UDP-GlcA analogs lacking the 6' carboxylic acid bind the enzyme but fail to trigger the conformational change, resulting in poor inhibition; and (ii) the uridine monophosphate moiety of the substrate

[*]**Corresponding Author**: Marcelo C. Sousa, Department of Biochemistry, 596 UCB, University of Colorado Boulder, Boulder, Colorado 80309, USA, Telephone: 303 735 4341, Fax: 303 492 8425, Marcelo.Sousa@colorado.edu.

[#]Current Address: Eli Lilly and Company, Lilly Corporate Center Indianapolis, IN 46285

[†]Current Address: Loxo at Lilly, 600 Tech Court, Louisville, CO 80027

Author Contributions

M.E. Mitchell: Conceptualization, Investigation, Methodology, Formal analysis, Visualization, Writing - Original Draft, Funding acquisition. P.Z. Gatzeva-Topalova: Conceptualization, Investigation, Formal analysis, Writing - Review & Editing. A.D. Bargmann: Investigation, Resources, Writing - Review & Editing. T. Sammakia: Conceptualization, Writing - Review & Editing, Supervision. M.C. Sousa: Conceptualization, Formal analysis, Visualization, Writing - Review & Editing, Supervision, Funding acquisition.

Accession Codes

Structure factors and structure coordinates have been deposited in the Protein Data Bank (PDB) under accession numbers: 8GJH (stArnA); and 8FTN (ecArnA_DH N492A). All other data are described in the manuscript and supporting information.

Supporting Information. Additional figures depicting the pathway responsible for the biosynthesis of [Ara4N]-Lipid-A; structure comparisons of ArnA from *Salmonella* Typhimurium, *E. coli* and human homologs; double reciprocal plots of ArnA_DH activity in the presence of UDP-Glc; experimental melting curves and details of method to estimate K_D; conformational change assay at high nucleotide concentrations; schemes of reactions catalyzed by human homologs of ArnA_DH; and table of crystallographic data collection and refinement (PDF).

Conflict of Interest Statement

The authors declare that they have no conflicts of interest with the contents of this article. Dr. Gatzeva-Topalova is an employee of Eli Lilly and Company and owns stocks/shares in the company. The work presented in this article was completed prior to Dr. Gatzeva-Topalova's Eli Lilly and Company employment and is not in any manner affiliated with Eli Lilly and Company. Dr. Sammakia is an employee of Eli Lilly and Company and owns stocks/shares in the company. The work presented in this article was completed prior to Dr. Sammakia's Eli Lilly and Company employment and is not in any manner affiliated with Eli Lilly and Company.

provides most of the ligand binding energy. Mutation of asparagine 492 to alanine (N492A) disrupts the ability of ArnA_DH to undergo the conformational change while retaining substrate binding, suggesting that N492 is involved in sensing the 6’ carboxylate in the substrate. These results identify the UDP-GlcA-induced conformational change in ArnA_DH as an essential mechanistic step in bacterial enzymes, providing a platform for selective inhibition.

Graphical Abstract

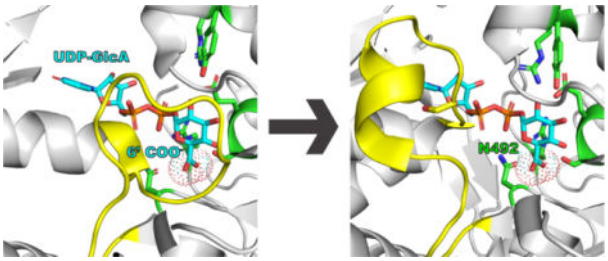

Keywords

antibiotic resistance; conformational change; enzyme structure; enzyme mechanism; enzyme inhibitor; polymyxin; lipid A modification

INTRODUCTION

Polymyxins are a family of cationic peptide antibiotics, of which polymyxin B and colistin are used to treat multidrug-resistant infections with Gram-negative bacteria. The mechanism of action of polymyxins involves electrostatic interaction with anionic phosphate groups in the lipid A moiety of lipopolysaccharide (LPS) in the Gram-negative outer membrane followed by membrane permeabilization, among other killing mechanisms.[1–9] Whereas their narrow therapeutic window reserves polymyxins to “last resort” usage, they are bactericidal and remain one of the few treatment options for infections with multidrug resistant Gram-negative bacteria.[6, 7, 10–14] As such, polymyxins are designated by the World Health Organization among the “Highest Priority Critically Important Antimicrobials for Human Medicine” for risk management of antimicrobial resistance.[15] Nevertheless, polymyxin resistance in clinical isolates is increasingly reported.[16–19]

The most prevalent mechanism of polymyxin resistance in *Pseudomonas* as well as *Klebsiella, Salmonella* and other *Enterobacteriaceae*, is the covalent modification of lipid A phosphates with cationic 4-amino arabinose (Ara4N). This modification reduces the negative charges on LPS, thus reducing polymyxin binding and conferring resistance to cationic peptide antibiotics.[20, 21] Biosynthesis of Ara4N and its transfer to lipid A requires seven enzymatic steps catalyzed by proteins encoded in the *arnBCADTEF* operon, which is widely distributed across human Gram-negative pathogens.[20, 21] All proteins encoded by this operon are essential for LPS modification and polymyxin resistance[22, 23] and, therefore, represent attractive targets for inhibitor development.

Ara4N is synthesized in the bacterial cytoplasm in two-steps using glucuronic acid attached to the soluble uridine diphosphate (UDP) carrier (SI Fig. S1). The first step of the transformation is catalyzed by the dehydrogenase domain of ArnA (ArnA_DH).[20–23] The Ara4N amine is then transiently formylated prior to transfer of the amino sugar to the lipid carrier undecaprenyl-phosphate (C55P) located in the inner membrane. This is followed by deformylation, flipping to the periplasmic side of the inner membrane, and finally transfer of Ara4N to lipid A. Most of the enzymes involved in this pathway have human homologues that catalyze similar chemistries, constituting a challenge for the development of selective inhibitors. However, ArnA_DH has a mechanism that sets it apart from its homologues and offers an opportunity for selective inhibition.[24]

ArnA is a hexameric protein encoded by the *arnBCADTEF* operon. Each monomer has two separable domains with distinct enzymatic activities.[24–27] The N-terminal domain is a transformylase (ArnA_TF) that catalyzes the transient formylation of UDP-Ara4N, whereas its C-terminal domain is a dehydrogenase (ArnA_DH) responsible for the first pathway-specific reaction of Ara4N-lipid A biosynthesis. ArnA_DH uses NAD^+ and UDP-GlcA as substrates, catalyzing the oxidative decarboxylation of UDP-GlcA to form UDP-4-keto-pentose, CO_2 and NADH (Scheme 1).

In the crystal structure of ligand-free *Escherichia coli* ArnA_DH (ecArnA_DH, PDB ID 1U9J), residues 500–509 define a loop (L1) that partially occludes the NAD^+ binding site, while residues 606–615 constitute a poorly ordered loop (L2) that could not be modeled (Fig. 1A).[26, 27] The structure of the full length ecArnA (PDB ID 1Z7E) in complex with UDP-GlcA and ATP (as an NAD^+ analog) reveals that ligand binding causes a large conformational change in the L1 loop. The conformational change results in an opening of the NAD^+ binding site, while the L1 loop folds into a short helix (H1) over UDP-GlcA "trapping" it in place (Fig. 1B). Ordering of the L2 loop into a short helix (H2) around the uridine moiety also contributes to the trapping of UDP-GlcA.[24]

ArnA_DH belongs to the extended short-chain dehydrogenase/reductase (SDR) superfamily, whose members are found across all domains of life.[28] The closest human homologs of ArnA_DH also catalyze NAD^+-dependent oxidation of a sugar nucleotide 4' hydroxyl and are involved in galactose metabolism,[29] protein glycosylation,[30] and the synthesis of proteoglycans and glycolipids.[31–33] Therefore, inhibitors resembling substrate or transition state analogs are likely to target both ArnA and its human homologs with little selectivity.

In this work, we investigate the ligand and enzyme features required for the ArnA_DH conformational change that is essential for activity. We present the crystal structure of *Salmonella* Typhimurium ArnA in complex with UDP-GlcA alone, which indicates that UDP-GlcA binding is sufficient to induce the conformational change. Sequence and structure comparisons reveal that only bacterial ArnA_DH orthologs, and none of the human homologs, have the structural elements required to undergo the ligand-induced conformational change, suggesting a venue for selective inhibition. Enzymatic assays show that the closely related substrate analog, UDP-Glucose (UDP-Glc) binds the enzyme with lower affinity than UDP-GlcA and is a poor inhibitor of the enzyme even at high concentrations. Functional probing demonstrates that UDP-Glc fails to trigger the

conformational change. UDP-Glc differs from UDP-GlcA in that it has a 6’ hydroxyl instead of a 6’ carboxylate, suggesting that sensing the carboxylate is essential for ArnA_DH conformational change and catalysis. We identify N492 as critical for sensing the presence of the 6’ carboxylate and triggering of the conformational change. We show that an N492A substitution precludes the conformational change even in the presence of UDP-GlcA. The N492A mutant has no enzymatic activity, despite retention of the native enzyme conformation as judged by determination of its crystal structure.

MATERIALS AND METHODS

Cloning and Protein Purification

The gene for *Salmonella enterica* serovar Typhimurium ArnA (stArnA, Uniprot: O52325) was amplified by PCR from genomic DNA using the following primers: sense primer −5’-GAA AGC CAC ATA TGA AAG CCG TTA TTT TTG C containing a NdeI site and antisense primer 5’-ACG TCA GAG CTC AAA CCG ACT TTC GTC ATG ATG containing a SacI site. The PCR product was digested with NdeI and SacI (New England BioLabs), gel purified, and ligated into an engineered variant of the pET28 vector. The resulting N-terminal His-tag fusion can be efficiently and specifically cleaved with the Tobacco etch virus (TEV) protease. The resulting plasmid was sequenced to confirm that no mutations had been introduced in the sequence.

E. coli Rosetta (DE3) cells were transformed with the plasmid. A 100 mL overnight culture from a single colony was used to inoculate 6 × 1 L Luria Broth (LB) medium supplemented with 50 μg/mL kanamycin. Cultures were grown at 37°C to OD_{600} of 0.6 and cooled on ice before induction with 0.4 mM isopropyl β-D-1-thiogalactopyranoside (IPTG). After incubation overnight at room temperature, cells were harvested by centrifugation at 6000 rpm for 10 min at 4 °C. The cell pellet was resuspended in 100 mL of lysis buffer containing 25 mM Tris-HCl pH 8.0, 5 mM 2-mercaptoethanol and 1 tablet of cOmplete™ EDTA-free Protease Inhibitor Cocktail (Roche). Lysis was achieved by sonication on ice. NaCl was added to a final concentration of 300 mM and cell debris removed by centrifugation at 16000 rpm for 30 min at 4 °C. The supernatant was then applied to 10 mL Ni-NTA column (Qiagen) previously equilibrated with buffer A (25 mM Tris-HCl pH 8.0, 5 mM 2-mercaptoethanol, 300 mM NaCl). The column was washed with 5 column volumes (CV) of buffer A containing 25 mM imidazole pH 8.0 and the protein eluted using a linear gradient of 25 – 300 mM imidazole in buffer A. Fractions containing the protein were pooled and loaded on a size exclusion column (HiLoad 26/60 Superdex 200, Amersham Pharmacia Biotech) equilibrated with 25 mM Tris-Cl pH 8.0, 150 mM KCl, 10 % glycerol, 1 mM EDTA pH 8.0, 5 mM 2-mercaptoethanol and eluted in the same buffer. Elution was monitored by measuring the absorption at 280 nm. The fractions containing protein were combined and the protein concentrated to approximately 8.2 mg/mL (Bio-Rad Protein Assay, Bio-Rad Laboratories). Protein was stored at −80 °C until needed.

The gene for the dehydrogenase domain of *E. coli* ArnA (Uniprot P77398, amino acids 314–660) was amplified from genomic DNA and cloned into a modified pET28 plasmid as described above for *Salmonella* ArnA, resulting in an N-terminal fusion to a TEV cleavable His-tag. *E. coli* BL-21 (DE3) cells were transformed with this plasmid and plated on

LB-agar with 50 μg/mL kanamycin. A single colony was picked for inoculation of 100 mL LB medium supplemented with 50 μg/mL kanamycin and the culture grown at 37 °C while agitated at 150 rpm overnight. A 5 mL aliquot of the overnight culture was used to inoculate 4 × 0.5 L LB supplemented with 50 μg/mL kanamycin. Cultures were grown at 37 °C and 150 rpm, until OD_{600} = 0.4 – 0.6. Cultures were then cooled to 4 °C by swirling in an ice bath. Expression was induced with 0.4 mM IPTG and the cultures incubated at 18 °C and 150 rpm overnight. Cells were harvested by centrifugation in a JLA8.1 rotor at 3800 rpm and 4 °C. Each pellet was resuspended in 25 mL of 10% glycerol, 25 mM Tris-HCl pH 8.0, 300 mM NaCl, 1 mg/mL lysozyme, 1 μL benzonase, and 1 tablet of cOmplete™ EDTA-free Protease Inhibitor Cocktail (Roche) per 50 mL. The cell resuspension was freeze-thawed and passed through a Emulsiflex C3 homogenizer three times to lyse the cells. The lysate was cleared by centrifugation at 15000 rpm in an SS-34 Sorvall rotor. The lysate was filtered through a 0.22 μm PVDF syringe filter and loaded onto a pre-packed Ni-NTA FastFlow column (Cytiva) equilibrated in binding buffer containing 25 mM Tris-HCl pH 8.0, 150 mM NaCl, 10% glycerol, 5 mM 2-mercaptoethanol. The column was washed with 10 CV of binding buffer and eluted with binding buffer supplemented with 300 mM imidazole on a linear gradient over 5 CV.

The fractions with ArnA_DH were pooled, filtered through a 0.2 μm membrane, and loaded on an HiLoad 26/60 Superdex 200 size exclusion column (Amersham Pharmacia Biotech) at 4 °C, pre-equilibrated in 100 mM KCl, 25 mM Tris-HCl pH 8.0, 5 mM 2-mercaptoethanol and eluted in the same buffer. Fractions containing ArnA_DH were dialyzed overnight against 25 mM Tris-HCl pH 8.0, 10% glycerol and 5 mM 2-mercaptoethanol to remove the salt, filtered through a 0.2 μm membrane, loaded on a MonoQ 5/50 GL column equilibrated in buffer C (25 mM Tris-HCl pH 8.0, 5 mM 2-mercaptoethanol, 10% glycerol) and eluted in two steps: first a linear gradient of 0–20% buffer D (25 mM Tris-HCl pH 8.0, 5 mM 2-mercaptoethanol, 10% glycerol, 1 M NaCl) over one CV, followed by another linear gradient of 20–100% buffer D over 15 CV. To cleave the His-tag, the fractions containing protein were pooled, TEV protease added in 1:20 TEV:ArnA_DH molar ratio, and the solution supplemented with dithiothreitol (DTT) to 10 mM. The TEV cleavage reaction was allowed to proceed overnight at 4 °C. The solution was then centrifuged, filtered through a 0.2 μm membrane, loaded on a Superdex 200 size exclusion column at 4 °C equilibrated in 25 mM Tris-HCl pH 8.0, 150 mM KCl, 5 mM 2-mercaptoethanol, 10% glycerol, and eluted with the same buffer. ArnA_DH containing fractions were pooled and concentrated to 10 mg/mL.

The *E. coli* ArnA_DH_N492A mutant was created by the QuikChange protocol (Agilent) using the pET28 plasmid containing the wild-type ArnA_DH with TEV-cleavable His-tag and the following primers: Sense- 5’ CTCTTCCGCCCGTTTGCCTGGATGGG Antisense- 5’-CCCATCCAGGCAAACGGGCGGAAGAG. ArnA_DH_N492A was purified as described above for the wild-type ArnA_DH.

Protein Crystallization, X-Ray Data Collection and Structure Determination

Large, single crystals of stArnA were obtained at 16 °C using the hanging drop method and a 1:1 ratio of protein (5 mg/mL supplemented with 3mM UDP-GlcA) to precipitant

consisting of 1.5 – 2.0 M ammonium sulfate and 0.1 M MES pH 6.75. Prior to X-ray data collection, the crystals were transferred to a cryo-protecting solution composed of mother liquor containing 10 % glycerol, soaked for 5 min, then moved to a 20% glycerol solution and soaked for an additional 5 min. Immediately after that, the crystals were flash cooled in a nitrogen stream. A data set was collected on beam line 8.2.2 at the Advanced Light Source in Berkeley.

ArnA_DH_N492A was crystalized at 4 °C using the hanging drop method and a 1:1 ratio of protein (5 mg/mL in 25 mM HEPES pH 7.5 and 50 mM NaCl) to precipitant consisting of 3.2 M NaCl, 0.1 M Bis-Tris-HCl pH 5.2. Prior to data collection, crystals were transferred to a cryo-protection solution of precipitant supplemented with 25% glycerol and frozen in a nitrogen stream. Data collection was carried out on a Rigaku HomeLab system with a sealed tube generator and a PILATUS HPAD detector at the Biomolecular X-ray Crystallography core facility (RRID: SCR_019310), Department of Biochemistry, University of Colorado Boulder. All crystallographic data were indexed and integrated with HKL2000.[34] Structure determination and refinement were carried out in Phenix.[35, 36] Data collection and refinement statistics are shown in SI Table S1.

ArnA_DH Activity Assay

Activity assays were carried out as previously described[24, 26, 27, 37]. Briefly, NADH formation was observed by measuring absorbance at 340 nm in a Corning UV transparent 96-well plate. Reaction volumes were 100 μL with buffer conditions of 25 mM Tris-HCl pH 8.0, 10 % glycerol, 150 mM KCl, and saturating NAD^+ at a concentration of 4 mM. The ArnA concentration was 300 nM. Reactions were initiated with the addition of UDP-GlcA at the noted concentrations. NADH formation was measured in a Tecan Infinite M200pro plate reader. The absorbance at 340 nm was plotted over time, and the slope of the linear region at each concentration was taken as the initial velocity. Initial velocities vs concentration of UDP-GlcA were plotted and fitted to a Michaelis-Menten equation using OriginLabs data analysis software to obtain K_M and V_{max} values.

Thermal Stability Shift Assay

Thermal Stability Shift Assays (TSA) were carried out in a BioRad CFX96 Real-Time PCR system. Each sample was 50 μL in volume, with a protein concentration of 5 μM and a SYPRO™ Orange dye concentration of 1X. Each ligand was tested in triplicate at the indicated concentrations. Sample buffer conditions were 10% glycerol, 25 mM Tris-HCl pH 8.0, 200 mM KCl and 5 mM 2-mercaptoethanol. Melting curves were collected between 25 °C and 85 °C using 0.5 °C increments, holding at each temperature for 10 seconds prior to collecting fluorescence readings. The FRET channel was selected because SYPRO™ Orange has a large separation between its excitation (472 nm) and emission (570 nm), making the FRET mode ideal for data collection. Apparent K_D values were calculated as previously described[38, 39] (SI Fig. S5).

NADH Binding to Monitor ArnA_DH Conformational Change

The NADH fluorescence spectral assays were conducted in a Corning UV transparent 96-well plate in a Tecan Infinite M200Pro plate reader using an excitation wavelength of 340

nm. Emission spectra were collected from 390 nm to 550 nm. Each well had a total of 100 μL assay mixture containing 9 μM protein, 6 μM NADH, 10% glycerol, 150 mM KCl, 25 mM Tris-HCl pH 8.0, and the indicated concentrations of UDP-GlcA or related ligand.

Preparation of UDP-Xylose and α-D-Glucuronate-1-Phosphate

UDP-xylose was enzymatically produced by oxidative decarboxylation of UDP-GlcA via catalysis by UDP-xylose synthase (UXS) from *Cryptococcus neoformans*.[40] UXS was cloned, expressed in *E. coli* BL21 (DE3) cells, and purified by metal-affinity and size exclusion chromatography as described above for ArnA_DH. A reaction containing 0.2 mg/mL UXS, 10 % glycerol, 150 mM KCl, 25 mM Tris-HCl pH 8.0, 100 mM UDP-GlcA and 2 mM NAD^+ was incubated overnight at room temperature. Protein was removed by ultrafiltration and the sample loaded on a MonoQ 5/50 GL column equilibrated with 1 mM ammonium acetate pH 4.0. Elution was performed with a 1 – 500 mM ammonium acetate pH 4 gradient over 6 CV. Fractions containing UDP-xylose were identified by mass spectrometry, pooled, and lyophilized.

The trisodium salt of α-D-glucuronate-1-phosphate was prepared using a modification of the procedure of Maruoka et al.[41] Briefly, α-D-glucose-1-phosphate disodium salt (250 mg, 822 μmol) was taken up in 4:4:1 water, saturated aqueous sodium bicarbonate, and t-butanol (11.7 mL). The solution was cooled to 0 °C and (2,2,6,6-tetramethylpiperidin-1-yl) oxy (TEMPO, 329 μmol, 0.4 eq) was added. Sodium hypochlorite (1.8 μL of a 7% solution, 2 eq) was added dropwise to the reaction mixture. Following 1.5 hours of incubation at room temperature, methanol (24 mL) was added to precipitate the desired product. The reaction mixture was transferred to a Falcon tube, and the precipitate was collected via centrifugation to provide α-D-glucuronate-1-phosphate trisodium salt which was dried under vacuum. The overall yield was 223 mg, 656 μmol, 80%.

RESULTS

The crystal structure of Salmonella ArnA reveals that UDP-glucuronic acid is sufficient to induce the ArnA_DH conformational change

As described above, the crystal structure of ecArnA in complex with UDP-GlcA and ATP (PDB ID 1Z7E) revealed a ligand-induced conformational change, whereby the L1 and L2 loops fold into short helices (H1 and H2) that open the NAD^+ binding site and “trap” the UDP-GlcA in its binding site (Fig. 1B and D)[24]. To test if UDP-GlcA binding to ArnA_DH is sufficient to trigger the conformational change in the substrate binding site, we sought to obtain a crystal structure of the enzyme in complex with UDP-GlcA. Single crystals of full length stArnA amenable to X-ray diffraction analysis were obtained in the presence of UDP-GlcA. The crystals diffracted to 3.6 Å resolution and belonged to space group P1, containing six ArnA protomers in the asymmetric unit. The structure was determined by molecular replacement using ecArnA (PDB ID 1Z7E) as a search model and was refined to a crystallographic R-factor = 0.218 (R-free = 0.267). Data collection and refinement statistics are shown in SI Table S1.

As expected, the stArnA structure is a hexamer arranged as a dimer of trimers with the ArnA_DH domains in the center (gray and black in Fig. 2A) and the ArnA_TF domains in the periphery (light and bright green in Fig. 2A). The hexamer structure of stArnA is very similar to that of ecArnA with an overall superposition RMSD of 1.4 Å (SI Fig. S2A). The structure of stArnA_TF domain is virtually identical to that of the *E. coli* ortholog, superimposing with an RMSD of 0.6 Å (SI Fig. S2B). Despite the limited resolution, the presence of UDP-GlcA in the stArnA_DH domain is clearly visible in a simulated annealing difference Fourier (Fobs-Fc) map (Fig. 2C). Similarly, simulated annealing omit maps allow the unambiguous tracing of residues 500–509 (Fig. 2D) and 606–615 (Fig. 2E) without model bias, indicating that they are in a helical conformation (H1 and H2). Therefore, stArnA_DH in complex with UDP-GlcA (Fig. 2B) is in the conformation previously observed in ligand-bound ecArnA_DH (Fig. 1B). The two ArnA_DH structures overlay with an RMSD of 0.5 Å (SI Fig. S2C). These results indicate that UDP-GlcA binding is sufficient to induce the structural transition that opens the NAD^+ binding site and traps the sugar nucleotide in its respective binding site. These results demonstrate that the ligand-induced conformational change in ArnA_DH is not unique to the *E. coli* protein.

Human homologs of ArnA_DH lack the structural elements involved in the conformational change

A central feature of the ArnA_DH conformational change is the transition of residues 500–509 from a loop that occludes the NAD^+ binding site in the apo form (L1), to a short helix (H1) upon UDP-GlcA binding (Fig. 1). To examine the conservation of the L1 loop in ArnA_DH across species, a BLAST[42] search of the Reference Sequence Select database was conducted. The search returned 564 sequences containing both transformylase and dehydrogenase domains, thus deemed to be ArnA orthologs. The sequences were aligned using Clustal Omega[43]. The polypeptide segment corresponding to the L1 loop was present in all orthologs without insertions or deletions and the sequence conservation is illustrated in Fig. 3A using Logos[44]. Overall, the L1 loop sequence is well conserved, with stArnA_DH D499, R505 and the GSSR motif (507–510) strictly conserved in all but the three most divergent sequences (from *Wigglesworthia*, *Kiloniella* and *Thorselia*) where the residues are partially conserved. The structure of ecArnA_DH with and without ligands reveals the importance of these residues in stabilizing the conformations of this segment. In the apo form of ecArnA_DH (Fig. 3B), a network of intraloop hydrogen bonds between side chains and main chain atoms — D499:S508; S508:D499; R510:A503 and R505 — stabilize the L1 loop conformation, while a hydrogen bond between N492 and S509 and a salt bridge between R505 and D347 help position this loop in the NAD^+ binding cleft. In the two independently refined structures of ecArnA_DH (PDB ID 1U9J[26] and PDB ID 2BLL[27]), the Phi/Psi angles of residue 507 put it in the disallowed region of the Ramachandran plot, consistent with its conservation as a glycine. Upon UDP-GlcA binding, loop L1 transitions to a helical conformation (H1, Fig. 1B and 2B). As shown in Fig. 3C, this ligand bound conformation is stabilized by a salt bridge between D499 and R510 in addition to the α-helical main chain hydrogen bonds. Furthermore, interactions between the side chains of S508 and E397, the guanidinium group of R400 and the carbonyl oxygen of I506, as well as packing of L501 in a hydrophobic pocket formed by I516, L517, V520, F649 and V653

help dock the H1 helix against the sugar nucleotide binding subdomain, thereby opening the NAD^+ binding site.

To explore if the structural features of ArnA_DH that allow it to undergo the L1 to H1 conformational change are conserved in its human homologs, a structure similarity search of the AlphaFold2 database[45] of human protein structures was carried out using ecArnA_DH as a search model. The top five hits were extended SDR family members that catalyze NAD(P)-dependent reactions on the 4' hydroxyl group of sugar nucleotides (SI Fig. S3), whereas other hits were SDR family members with non-sugar nucleotide substrates. A structure-based sequence alignment of ArnA_DH and the top 5 human homologs (UDP-GlcA decarboxylase, dTDP-Glc 4,6-dehydratase, UDP-Glc epimerase, GDP-mannose 4,6-dehydratase, and GDP-fucose synthase) reveals that the ArnA_DH L1 loop is missing in the human enzymes (Fig. 3D). Furthermore, a structure superposition shows that only ArnA_DH has a loop that occupies the NAD(P) binding cleft (Fig. 3E and SI Fig. S3). This analysis suggests that the ArnA_DH conformational change is a unique feature of the bacterial enzymes, distinguishing them from human homologs.

The 6' carboxylate of UDP-GlcA is critical for triggering the conformational change

The NAD^+-dependent oxidative decarboxylation of UDP-GlcA catalyzed by ArnA_DH (Scheme 1) can be monitored by measuring the production of NADH spectrophotometrically at 340 nm.[24, 26, 27, 37] We anticipated that UDP-Glc would be an effective competitive inhibitor for ArnA_DH as it is structurally similar to the substrate UDP-GlcA, with a 6' alcohol replacing the carboxylate (Fig. 4A). However, the presence of UDP-Glc had little effect on the activity of ArnA_DH. UDP-Glc concentrations of up to 10 mM resulted in only a 2.5-fold increase in the apparent K_M for UDP-GlcA (Fig. 4B and SI Fig. S4).

Considering the weak inhibition, we implemented a fluorescence thermal shift assay with SYPRO™ Orange to quantify binding of UDP-GlcA and analogs, such as UDP-Glc, to ArnA_DH.[39, 46, 47] Ligand binding was assessed from the shift in melting temperature in the presence of the ligand relative to the melting temperature in its absence. Using established mathematical models[38, 39] to estimate ligand binding affinities from the thermal shift data (see Experimental Procedures and SI Fig. S5 for details), we obtained apparent $K_D \pm$ SD values of 22 ± 5 μM for UDP-GlcA and 895 ± 97 μM for UDP-Glc at 25 °C. As UDP-Glc clearly binds ArnA_DH, albeit with lower affinity than the substrate UDP-GlcA, we next investigated if UDP-Glc was able to induce the conformational change in ArnA_DH required for catalytic activity.

We developed an approach to monitor the ArnA conformational change based on binding of NADH to ArnA_DH. NADH which cannot support oxidative catalysis by ArnA_DH, is intrinsically fluorescent and often displays a blue shift and an increase in fluorescence quantum yield when bound to protein.[48] As shown in Fig. 4D, in the absence of UDP-GlcA, ArnA_DH is in the apo conformations with loop L1 occluding the NAD^+ binding site, which prevents binding of NADH and results in low intrinsic NADH fluorescence (Fig. 4D black curve). However, upon addition of UDP-GlcA, ArnA_DH undergoes the conformational change that opens the NAD^+ binding site allowing NADH binding, which is accompanied by an increase in fluorescence quantum yield and a blue shift in the maxima (Fig. 4D blue

curve). In contrast to the substrate UDP-GlcA, addition of UDP-Glc results in low intrinsic NADH fluorescence and no blue shift (Fig. 4D pink curve). Even addition of 10 mM UDP-Glc to ArnA does not result in NADH binding and thus its fluorescence remains low (SI Fig. S6). We thus conclude that UDP-Glc does not induce the ArnA_DH conformational change.

The 6' sugar carbon in the substrate UDP-GlcA is part of a carboxylate (Fig. 4A) and therefore has sp2 hybridization with planar geometry. Conversely, the 6' carbon in UDP-glucose is a primary alcohol with sp3 hybridization and tetrahedral geometry. As the substituents in the 6' alcohol of UDP-glucose are hydrogens, it appears unlikely that steric hindrance due to the tetrahedral geometry would affect binding of the sugar moiety to ArnA_DH and prevent the conformational change. Nevertheless, we also tested the binding of UDP-xylose, which lacks the 6' carbon altogether (Fig. 5A), to rule out the possibility of steric hindrance. As judged by the thermal shift assay (Fig. 5B), UDP-xylose binds ArnA_DH with an apparent K_D of 633 ± 116 μM, similar to that of UDP-glucose, suggesting that the 6' alcohol in UDP-Glc does not experience substantial steric clash upon binding. We also tested if UDP-xylose can induce the conformational change using the NADH binding assay. As shown in Fig. 5C, intrinsic NADH fluorescence remains low and red shifted in the presence of ArnA_DH and UDP-Xyl (purple curve) indicating that this sugar nucleotide fails to induce the conformational change. Taken together, these results suggest that the 6' carboxylate in UDP-GlcA is required for the conformational change in ArnA_DH and for its enzyme activity.

The UMP moiety provides most of the substrate UDP-GlcA binding energy

Previous studies with enzymes that use sugar nucleotides as substrates reveal that the nucleotide moiety often drives substrate binding while the sugar contributes relatively little binding energy.[49] To test if this is also the case for ArnA_DH, we "divided" the substrate into uridine monophosphate (UMP) and glucuronic acid-1-phosphate (GlcA-1P) (Fig. 5A) and tested their binding affinity for ArnA_DH using the thermal stability shift assay. As shown in Fig. 5B, GlcA-1P binding is undetectable (bright and dark green curves), while UMP binds ArnA_DH (orange curve) with an apparent K_D of 594 ± 135 μM, similar to that of UDP-Glc (SI Fig. S5). These results suggest that the nucleotide moiety provides most of the binding affinity of the UDP-GlcA substrate for the protein.

Our results suggest that the 6' carboxylate in UDP-GlcA is required to induce the conformational change in ArnA_DH. Consistent with this hypothesis, UMP was unable to trigger the conformation change in the enzyme as judged by NADH fluorescence emission spectra (Fig. 5C orange curve). Similarly, GlcA-1P also fails to induce the conformational change and intrinsic NADH fluorescence is unaffected by the presence of ArnA_DH and GlcA-1P (Fig. 5C green curve). This is consistent with the undetectable binding of GlcA-1P to the enzyme (Fig. 5B). We also tested if addition of UMP and GlcA-1P together was able to induce the ArnA_DH conformational change. As shown in Fig. 5D, NADH fluorescence remains low and red shifted upon simultaneous addition of the two UDP-GlcA "halves" (UMP and GlcA-1P, gold curve). In contrast, the intact substrate (UDP-GlcA, blue curve) triggers the conformational change and allows NADH binding with the corresponding

increase in quantum yield and blue shift in fluorescence. Taken together, these experiments suggest that UMP provides most of the binding energy for the substrate while the glucuronic acid provides the critical 6' carboxylate required for the L1 to H1 conformational change in ArnA_DH.

N492 is a necessary residue for the conformational change in ArnA_DH

Our data imply that ArnA_DH has a mechanism to sense the presence of the 6' carboxylate of the substrate. Structure and sequence similarity analysis of bacterial ArnA_DH orthologs and comparison to related SDR enzymes allow for the identification of amino acid residues that interact with UDP-GlcA and are conserved in ArnA_DH but diverge in related SDR enzymes. Fig. 6 displays the active site of ecArnA_DH as structures are available in both apo and ligand bound forms, and determined at the highest resolution. Nevertheless, the active site residues and protein conformations of ligand-bound *E. coli* and *Salmonella* ArnA_DH are conserved. Among the active site residues, N492 appears as the most likely candidate for sensing the UDP-GlcA 6' carboxylate. In the apo form of ecArnA_DH, the side chain of N492 interacts with S509 located in the L1 loop that occludes the NAD^+ binding site (Fig. 6A). However, in the ligand-bound structures of ArnA_DH, the N492 side chain is close to the UDP-GlcA 6' carboxylate and no longer in contact with S509, whose β-hydroxyl shifts 8.4 Å away as a result of the L1 loop conformational change (Fig. 6B). To test the importance of this residue, we mutated it to an alanine in the ecArnA_DH and evaluated its effect on ligand binding and activity.

We first tested the ability of ArnA_DH_N492A to undergo the UDP-GlcA-induced conformational change. As shown in Fig. 7A, there is little change in the intrinsic NADH fluorescence upon addition of ArnA_DH_N492A and UDP-GlcA in concentrations as high as 10 mM (cyan curve), in stark contrast to the increase and blue shift in fluorescence observed for wild type ArnA_DH (blue curve). Therefore, ArnA_DH_N492A does not undergo the UDP-GlcA-induced conformational change. Consistent with these results, ArnA_DH_N492A is inactive suggesting that residue N492 is important to trigger the conformational change necessary for activity. However, these results could also be due to the N492A mutation impairing UDP-GlcA binding to the enzyme. The thermal stability shift assay was then used to evaluate UDP-GlcA binding to ArnA_DH_N492A. As shown in Fig. 7B, the substrate strongly stabilizes the mutant enzyme (cyan curve), binding with an apparent K_D of 36 ± 7 μM, similar to that of wild type ArnA_DH. This indicates that binding of UDP-GlcA is not significantly disrupted in ArnA_DH_N492A.

To rule out misfolding as the reason for loss of activity/conformational change in the mutant, we crystalized ArnA_DH_N492A under the same conditions previously described for wild type ArnA_DH.[26] An X-ray diffraction dataset to 2.8 Å resolution was collected from ArnA_DH_N492A and the structure determined by molecular replacement using the wild-type ecArnA_DH apo structure (PDB ID 1U9J) as the search model. After simulated annealing to remove model bias, the mutant model was refined to a crystallographic R-factor = 0.225 (R-free = 0.263). The data collection and refinement statistics are reported in SI Table S1. The ecArnA_DH_N492A structure is virtually identical to the wild-type enzyme, with the two structures superimposing with an RMDS = 0.27Å (all atoms) indicating no

misfolding due to the mutation. Taken together, these results show that ArnA_DH_N492A folds into the native conformation and binds UDP-GlcA similarly to the wild-type enzyme yet is unable to undergo the conformational change. This suggests that N492 is important for sensing the 6' carboxylate on UDP-GlcA or for another essential step leading to a conformational change in ArnA_DH.

DISCUSSION

The ArnABCDEFT enzymes are essential for the Ara4N-lipid A modification (SI Fig. S1) and for polymyxin resistance in Gram-negative pathogens. These enzymes are thus attractive targets for development of inhibitors that may be used as adjuvants to increase polymyxin efficacy. However, most of the enzymes have closely related human homologs with conserved active sites that catalyze similar reactions, complicating the development of inhibitors selective for the bacterial proteins. Nevertheless, the study of the enzymes' reaction mechanism may allow identification of unique features that enable selective inhibition.

The C-terminal, dehydrogenase domain of ArnA catalyzes the first pathway-specific reaction in the biosynthesis of Ara4N-lipid A. The structure of *Salmonella enterica* serovar Typhimurium ArnA in complex with UDP-GlcA presented here shows that UDP-GlcA binding is sufficient to induce the conformational change that had previously been observed for the *E. coli* enzyme in complex with both UDP-GlcA and ATP. This observation supports a previously proposed ordered substrate binding mechanism[24], where UDP-GlcA binds first and induces the conformational change allowing NAD^+ binding. Here, we used NADH as an intrinsically fluorescent, isosteric probe for NAD^+ binding to directly test this hypothesis. The NADH binding experiments confirm an ordered substrate binding mechanism in ArnA, with no cofactor bound to the enzyme in the absence of UDP-GlcA (Fig. 4D). Therefore, the UDP-GlcA-induced conformational change is an essential step in the reaction mechanism, that allows binding of the second substrate, NAD^+.

ArnA_DH sequence similarity analyses indicate that the L1 loop which partially occludes the NAD^+ binding site in the apo enzyme and which changes conformation upon UDP-GlcA binding, is well conserved in bacterial orthologs (Fig. 3A). Furthermore, residues that are strictly conserved in all but the three most distant orthologs play key roles in the structural stabilization of the apo L1 loop and/or the H1 helix after the conformational change (Fig. 3B and C). This indicates that the UDP-GlcA-induced conformational change is a conserved mechanistic step in ArnA_DHs across bacterial species, as experimentally observed previously for the *E. coli*[24] and here for the *Salmonella* enzymes.

No human protein catalyzes exactly the same reaction as the one catalyzed by ArnA_DH. Nevertheless, structure similarity searches identified five human proteins that are closely related to ArnA_DH and catalyze similar chemistries. Human UDP-GlcA decarboxylase synthesizes UDP-xylose, an essential xylose donor for the biosynthesis of proteoglycans[31, 32] and α-dystroglycan.[33] This enzyme shares the first and second chemical steps with ArnA_DH. UDP-GlcA decarboxylase catalyzes the NAD^+-dependent oxidation of the 4' hydroxyl of UDP-GlcA with formation of NADH, followed by decarboxylation (SI Fig.

S7A). The resulting UDP-4-keto-6-deoxy-glucose is then reduced by NADH to generate UDP-xylose. Therefore, in contrast to ArnA_DH which consumes NAD^+ and releases NADH, UDP-GlcA decarboxylase uses NAD^+ as a coenzyme that is not consumed in the reaction and remains tightly bound to the enzyme. Consequently, UDP-GlcA decarboxylase purifies with NAD^+ stoichiometrically bound.[37] The same is true for the reactions catalyzed by three other human homologs of ArnA_DH: UDP-glucose epimerase (GALE), central to the Leloir pathway of galactose metabolism, protein glycosylation, and the synthesis of proteoglycans and glycolipids;[29, 50] GDP-mannose 4,6-dehydratase in the pathway for biosynthesis of the essential sugar donor GDP-fucose, whose deficiency leads to blood disorders[30] and significantly impacts cancer biology;[51–53] and dTDP-glucose 4,6-dehydratase with unknown function in humans but whose mutation impairing activity causes Catel-Manzke syndrome.[54] These three enzymes catalyze $NAD(P)^+$-dependent oxidation of a sugar nucleotide 4' hydroxyl but retain the resulting NAD(P)H to catalyze a subsequent reductive step (SI Fig. S7B–D). Structure-based sequence alignments, as well as structure superposition of ligand-free AlphaFold models of these enzymes with ArnA_DH, indicate that they all lack the L1 loop segment (Fig. 3C and D), consistent with their having the nicotinamide coenzyme "permanently" bound. The crystal structures of three of these human enzymes, purified with their NAD(P) coenzyme bound, have been experimentally determined and are essentially identical to their ligand-free AlphaFold models (SI Fig. S3). One additional human homolog of ArnA_DH, GDP-fucose synthase, catalyzes the last step in UDP-fucose synthesis which involves epimerization of GDP-4-keto-6-deoxy-mannose followed by the NADPH-dependent reduction of the 4' ketone to yield GDP-fucose and $NADP^+$ (SI Fig. S7E). The enzyme uses NADPH as a substrate and releases $NADP^+$ as a product. However, this enzyme also lacks the L1 loop amino acids. The enzyme's AlphaFold model as well as the structure of the ligand-free *E. coli* ortholog reveal an open $NADP^+$/H binding site (Fig. 3D, E and SI Fig. S3F). Therefore, only bacterial ArnA_DH orthologs, and none of its close human homologs, have the structural features to undergo the sugar nucleotide-induced conformational change observed in ArnA_DH.

The NADH binding experiments in the presence of UDP-Glc and UDP-Xyl indicate that the 6' carboxylate in UDP-GlcA is critical to the substrate binding site conformational change. Williams et al.[27], previously observed that ArnA_DH was unable to produce NADH in the presence of UDP-Glc despite its similarity to UDP-GlcA and the expectation that it would fit in the binding site. They proposed that this was due to the oxidative step (4' hydride transfer to NAD^+) having an unfavorable free energy and thus not occurring in the absence of the essentially irreversible decarboxylation step. Whereas this is still possible, our results indicate that UDP-Glc does not trigger the conformational change and therefore NAD^+ cannot bind and no oxidation can occur.

The 6' carboxylate of UDP-GlcA is critical for the conformational change in ArnA_DH. However, it is possible that analogs lacking this functional group may induce the structural transition. Polizzi et al.[37] reported that under certain conditions ArnA_DH can produce small amounts of UDP-xylose from its products UDP-4-keto-pentose and NADH. They suggest that this results from "rebinding" of the products to the enzyme and a slow reduction of the 4' ketone to yield UDP-xylose. Rebinding would imply that UDP-4-keto-pentose is able to trigger the conformational change despite lacking a 6' carboxylate. However, we note

that the experiments were carried out by allowing a standard UDP-GlcA + NAD^+ ArnA_DH reaction to proceed to completion, such that UDP-GlcA is depleted and UDP-4-keto-pentose and NADH accumulate. It is therefore possible that under such conditions UDP-Xyl is formed by ArnA_DH that has not released UDP-4-keto-pentose and thus the structure has not reset to the apo conformation. A direct test of the ability of UDP-4-keto-pentose to induce the conformational change is contingent upon the synthesis and purification of this sugar nucleotide.

The thermal stability shift assay employed to assess ligand binding[38, 46, 47] reports on protein thermal unfolding that is typically irreversible.[39] Nevertheless, derivation of K_D values using thermodynamic models, despite the irreversible nature of thermal denaturation, has been previously discussed and relies on the assumption that the irreversible thermal aggregation is slow compared to the interconversion of folded and unfolded species.[55–60] Additionally, the K_D calculation requires knowledge or estimation of the ligand binding enthalpy, ΔH. As this parameter is typically unavailable, fixed values of −15 kcal/mol are often used in the literature as originally suggested by Pantoliano et al.[39] However we used an estimate of −5 kcal/mol as Lo et al.[38] have shown that this value is more appropriate and results in K_D values that correlate well with those measured by ITC for a set of reference cases. Using this approach, we calculated apparent K_D values for the purpose of comparing relative affinities of UDP-GlcA and its analogs and fragments (SI Fig. S5). The experiments show that UDP-GlcA has an apparent K_D that is consistent with the K_M estimated from the activity assays. Furthermore, the ~30–40-fold increase in apparent K_D for UDP-Xyl and UDP-Glc compared to UDP-GlcA is consistent with the loss of a salt bridge between the 6’ carboxylic acid and ArnA_DH (approximately 4 kcal/mol). The apparent K_D for UMP was similar to that of UDP-Glc, while GlcA-1P binding was not detectable, suggesting that the UMP moiety provides most of the ligand binding energy.

The observation that, among the tested compounds, only UDP-GlcA was able to trigger the ArnA_DH conformational change, suggests that the enzyme has a mechanism for “sensing” the 6’ carboxylic acid on the substrate. Residue N492, which is conserved in ArnA_DH orthologs, is positioned to interact with the 6’ carboxylate of UDP-GlcA. Mutation of N492 to alanine abolished the ability of the substrate to trigger the conformational change indicating that the residue is indeed important in the mechanism. Consistent with its inability to undergo the conformational change, ArnA_DH-N492A is inactive. As the N492 residue is involved in stabilizing the conformation of the L1 loop (Fig. 3B) it could have been predicted that its mutation to alanine would destabilize the L1 conformation, perhaps resulting in the loop no longer occluding the NAD^+ binding site. However, a network of additional interactions stabilizes the L1 loop conformation in the apo form (Fig. 3B). It is therefore not surprising that the loss of the N492:S509 interaction does not disrupt the native apo structure as confirmed by the mutant crystal structure.

CONCLUSION

Our results identify the substrate induced conformational change in ArnA_DH as a unique feature of the bacterial enzyme setting it apart from its human homologs, despite their structural and catalytic similarity. Whereas UDP-GlcA binding site ligands that are unable

to induce the conformational change may be good competitive inhibitors, they may not be selective for ArnA_DH given the similarity between bacterial and human enzymes. Conversely, ligands that trigger the conformational change, which is unique to bacterial enzymes, may be trapped in the ArnA_DH active site resulting in effective and selective inhibition. We, therefore, propose that the ArnA_DH conformational change could be targeted for the development of selective inhibitors. To this end, the 6' carboxylate of the sugar appears critical for triggering the conformational change although the sugar itself appears to provide limited binding energy to the native substrate. The NADH binding assay provides a simple and accessible way to screen for compounds that trigger the ArnA_DH conformational change while the thermal shift assay conveniently evaluates their relative affinities. Small molecules that trigger the ArnA_DH conformational change might be trapped in the UDP-GlcA binding site and would likely be selective for ArnA over the structurally related human enzymes.

Supplementary Material

Refer to Web version on PubMed Central for supplementary material.

ACKNOWLEDGEMENTS

We thank Wesley Beckham for assistance with the NADH binding assay and Annette Erbse for assistance and training in the use of the Shared Instruments Pool (RRID: SCR_018986) of the Department of Biochemistry at the University of Colorado Boulder, in particular the centrifuges and the Emulsiflex C3 homogenizer.

Funding Sources

This material is based in part on work supported by the National Science Foundation Graduate Research Fellowship Program under grant No. 1650115, and by a National Institute of General Medical Science "Signaling and Cellular Regulation Training Grant" No. T32 GM008759 to M.E.M; as well as a National Institute of Allergy and Infectious Diseases grant AI060841 to M.C.S. Any opinions, findings, conclusions, or recommendations expressed in this material are those of the authors and do not necessarily reflect the views of the National Science Foundation. The content is solely the responsibility of the authors and does not necessarily represent the official views of the National Institutes of Health.

REFERENCES

[1]. Shai Y (1999) Mechanism of the binding, insertion and destabilization of phospholipid bilayer membranes by alpha-helical antimicrobial and cell non-selective membrane-lytic peptides, Biochim Biophys Acta 1462, 55–70. [PubMed: 10590302]

[2]. Matsuzaki K (1999) Why and how are peptide-lipid interactions utilized for self-defense? Magainins and tachyplesins as archetypes, Biochim Biophys Acta 1462, 1–10. [PubMed: 10590299]

[3]. Li Z, and Velkov T (2019) Polymyxins: Mode of Action, Adv Exp Med Biol 1145, 37–54. [PubMed: 31364070]

[4]. Lee TH, Hall KN, and Aguilar MI (2016) Antimicrobial Peptide Structure and Mechanism of Action: A Focus on the Role of Membrane Structure, Curr Top Med Chem 16, 25–39. [PubMed: 26139112]

[5]. Rashid R, Veleba M, and Kline KA (2016) Focal Targeting of the Bacterial Envelope by Antimicrobial Peptides, Front Cell Dev Biol 4, 55. [PubMed: 27376064]

[6]. Scocchi M, Mardirossian M, Runti G, and Benincasa M (2016) Non-Membrane Permeabilizing Modes of Action of Antimicrobial Peptides on Bacteria, Curr Top Med Chem 16, 76–88. [PubMed: 26139115]

[7]. Sharma S, Sahoo N, and Bhunia A (2016) Antimicrobial Peptides and their Pore/Ion Channel Properties in Neutralization of Pathogenic Microbes, Curr Top Med Chem 16, 46–53. [PubMed: 26139119]

[8]. Yang L, Weiss TM, Lehrer RI, and Huang HW (2000) Crystallization of antimicrobial pores in membranes: magainin and protegrin, Biophys J 79, 2002–2009. [PubMed: 11023904]

[9]. Deris ZZ, Swarbrick JD, Roberts KD, Azad MA, Akter J, Horne AS, Nation RL, Rogers KL, Thompson PE, Velkov T, and Li J (2014) Probing the penetration of antimicrobial polymyxin lipopeptides into gram-negative bacteria, Bioconjug Chem 25, 750–760. [PubMed: 24635310]

[10]. Li J, Nation RL, Turnidge JD, Milne RW, Coulthard K, Rayner CR, and Paterson DL (2006) Colistin: the re-emerging antibiotic for multidrug-resistant Gram-negative bacterial infections, Lancet Infect Dis 6, 589–601. [PubMed: 16931410]

[11]. Michalopoulos A, and Papadakis E (2010) Inhaled anti-infective agents: emphasis on colistin, Infection 38, 81–88. [PubMed: 20191398]

[12]. Xu L, Sun X, and Ma X (2017) Systematic review and meta-analysis of mortality of patients infected with carbapenem-resistant Klebsiella pneumoniae, Ann Clin Microbiol Antimicrob 16, 18. [PubMed: 28356109]

[13]. Ramos-Castaneda JA, Ruano-Ravina A, Barbosa-Lorenzo R, Paillier-Gonzalez JE, Saldana-Campos JC, Salinas DF, and Lemos-Luengas EV (2018) Mortality due to KPC carbapenemase-producing Klebsiella pneumoniae infections: Systematic review and meta-analysis: Mortality due to KPC Klebsiella pneumoniae infections, J Infect 76, 438–448. [PubMed: 29477802]

[14]. Gilbert LJ, Li P, Murray CK, Yun HC, Aggarwal D, Weintrob AC, Tribble DR, and Program IDCR (2016) Multidrug-resistant gram-negative bacilli colonization risk factors among trauma patients, Diagnostic Microbiology and Infectious Disease 84, 358–360. [PubMed: 26867965]

[15]. Organization WH (2019) Critically important antimicrobials for human medicine, 6th revision, 6th Revision ed.

[16]. Alvarez Lerma F, Munoz Bermudez R, Grau S, Gracia Arnillas MP, Sorli L, Recasens L, and Mico Garcia M (2017) Ceftolozane-tazobactam for the treatment of ventilator-associated infections by colistin-resistant Pseudomonas aeruginosa, Rev Esp Quimioter 30, 224–228. [PubMed: 28361526]

[17]. Cheng YH, Lin TL, Pan YJ, Wang YP, Lin YT, and Wang JT (2015) Colistin resistance mechanisms in Klebsiella pneumoniae strains from Taiwan, Antimicrob Agents Chemother 59, 2909–2913. [PubMed: 25691646]

[18]. Jayol A, Nordmann P, Brink A, and Poirel L (2015) Heteroresistance to colistin in Klebsiella pneumoniae associated with alterations in the PhoPQ regulatory system, Antimicrob Agents Chemother 59, 2780–2784. [PubMed: 25733503]

[19]. Jayol A, Poirel L, Brink A, Villegas MV, Yilmaz M, and Nordmann P (2014) Resistance to colistin associated with a single amino acid change in protein PmrB among Klebsiella pneumoniae isolates of worldwide origin, Antimicrob Agents Chemother 58, 4762–4766. [PubMed: 24914122]

[20]. Needham BD, and Trent MS (2013) Fortifying the barrier: the impact of lipid A remodelling on bacterial pathogenesis, Nat Rev Microbiol 11, 467–481. [PubMed: 23748343]

[21]. Olaitan AO, Morand S, and Rolain JM (2014) Mechanisms of polymyxin resistance: acquired and intrinsic resistance in bacteria, Front Microbiol 5, 643. [PubMed: 25505462]

[22]. Gunn JS, Ryan SS, Van Velkinburgh JC, Ernst RK, and Miller SI (2000) Genetic and functional analysis of a PmrA-PmrB-regulated locus necessary for lipopolysaccharide modification, antimicrobial peptide resistance, and oral virulence of Salmonella enterica serovar typhimurium, Infect Immun 68, 6139–6146. [PubMed: 11035717]

[23]. Yan A, Guan Z, and Raetz CR (2007) An undecaprenyl phosphate-aminoarabinose flippase required for polymyxin resistance in Escherichia coli, J Biol Chem 282, 36077–36089. [PubMed: 17928292]

[24]. Gatzeva-Topalova PZ, May AP, and Sousa MC (2005) Structure and mechanism of ArnA: conformational change implies ordered dehydrogenase mechanism in key enzyme for polymyxin resistance, Structure 13, 929–942. [PubMed: 15939024]

[25]. Gatzeva-Topalova PZ, Andrew P, and Sousa MC (2005) Crystal structure and mechanism of the Escherichia coli ArnA (PmrI) transformylase domain. An enzyme for lipid A modification with 4-amino-4-deoxy-L-arabinose and polymyxin resistance, Biochemistry 44, 5328–5338. [PubMed: 15807526]

[26]. Gatzeva-Topalova PZ, May AP, and Sousa MC (2004) Crystal structure of Escherichia coli ArnA (PmrI) decarboxylase domain. A key enzyme for lipid A modification with 4-amino-4-deoxy-L-arabinose and polymyxin resistance, Biochemistry 43, 13370–13379. [PubMed: 15491143]

[27]. Williams GJ, Breazeale SD, Raetz CR, and Naismith JH (2005) Structure and function of both domains of ArnA, a dual function decarboxylase and a formyltransferase, involved in 4-amino-4-deoxy-L-arabinose biosynthesis, J Biol Chem 280, 23000–23008. [PubMed: 15809294]

[28]. Jornvall H, Hedlund J, Bergman T, Oppermann U, and Persson B (2010) Superfamilies SDR and MDR: from early ancestry to present forms. Emergence of three lines, a Zn-metalloenzyme, and distinct variabilities, Biochem Biophys Res Commun 396, 125–130. [PubMed: 20494124]

[29]. Conte F, van Buuringen N, Voermans NC, and Lefeber DJ (2021) Galactose in human metabolism, glycosylation and congenital metabolic diseases: Time for a closer look, Biochim Biophys Acta Gen Subj 1865, 129898. [PubMed: 33878388]

[30]. Becker DJ, and Lowe JB (2003) Fucose: biosynthesis and biological function in mammals, Glycobiology 13, 41R–53R.

[31]. Silbert JE, and Sugumaran G (2002) Biosynthesis of chondroitin/dermatan sulfate, IUBMB Life 54, 177–186. [PubMed: 12512856]

[32]. Li JP, and Kusche-Gullberg M (2016) Heparan Sulfate: Biosynthesis, Structure, and Function, Int Rev Cell Mol Biol 325, 215–273. [PubMed: 27241222]

[33]. Inamori K, Yoshida-Moriguchi T, Hara Y, Anderson ME, Yu L, and Campbell KP (2012) Dystroglycan function requires xylosyl- and glucuronyltransferase activities of LARGE, Science 335, 93–96. [PubMed: 22223806]

[34]. Otwinowski Z, and Minor W (1997) Processing of X-ray diffraction data collected in oscillation mode, Methods in Enzymology 276, 307–326. [PubMed: 27754618]

[35]. Adams PD, Afonine PV, Bunkoczi G, Chen VB, Davis IW, Echols N, Headd JJ, Hung LW, Kapral GJ, Grosse-Kunstleve RW, McCoy AJ, Moriarty NW, Oeffner R, Read RJ, Richardson DC, Richardson JS, Terwilliger TC, and Zwart PH (2010) PHENIX: a comprehensive Python-based system for macromolecular structure solution, Acta Crystallogr D Biol Crystallogr 66, 213–221. [PubMed: 20124702]

[36]. Liebschner D, Afonine PV, Baker ML, Bunkoczi G, Chen VB, Croll TI, Hintze B, Hung LW, Jain S, McCoy AJ, Moriarty NW, Oeffner RD, Poon BK, Prisant MG, Read RJ, Richardson JS, Richardson DC, Sammito MD, Sobolev OV, Stockwell DH, Terwilliger TC, Urzhumtsev AG, Videau LL, Williams CJ, and Adams PD (2019) Macromolecular structure determination using X-rays, neutrons and electrons: recent developments in Phenix, Acta Crystallogr D Struct Biol 75, 861–877. [PubMed: 31588918]

[37]. Polizzi SJ, Walsh RM Jr., Peeples WB, Lim JM, Wells L, and Wood ZA (2012) Human UDP-alpha-D-xylose synthase and Escherichia coli ArnA conserve a conformational shunt that controls whether xylose or 4-keto-xylose is produced, Biochemistry 51, 8844–8855. [PubMed: 23072385]

[38]. Lo MC, Aulabaugh A, Jin G, Cowling R, Bard J, Malamas M, and Ellestad G (2004) Evaluation of fluorescence-based thermal shift assays for hit identification in drug discovery, Anal Biochem 332, 153–159. [PubMed: 15301960]

[39]. Pantoliano MW, Petrella EC, Kwasnoski JD, Lobanov VS, Myslik J, Graf E, Carver T, Asel E, Springer BA, Lane P, and Salemme FR (2001) High-density miniaturized thermal shift assays as a general strategy for drug discovery, J Biomol Screen 6, 429–440. [PubMed: 11788061]

[40]. Bar-Peled M, Griffith CL, and Doering TL (2001) Functional cloning and characterization of a UDP- glucuronic acid decarboxylase: the pathogenic fungus Cryptococcus neoformans elucidates UDP-xylose synthesis, Proc Natl Acad Sci U S A 98, 12003–12008. [PubMed: 11593010]

[41]. Maruoka H, Jayasekara MP, Barrett MO, Franklin DA, de Castro S, Kim N, Costanzi S, Harden TK, and Jacobson KA (2011) Pyrimidine nucleotides with 4-alkyloxyimino and terminal

tetraphosphate delta-ester modifications as selective agonists of the P2Y(4) receptor, J Med Chem 54, 4018–4033. [PubMed: 21528910]

[42]. Altschul SF, Madden TL, Schaffer AA, Zhang J, Zhang Z, Miller W, and Lipman DJ (1997) Gapped BLAST and PSI-BLAST: a new generation of protein database search programs, Nucleic Acids Res 25, 3389–3402. [PubMed: 9254694]

[43]. Sievers F, Wilm A, Dineen D, Gibson TJ, Karplus K, Li W, Lopez R, McWilliam H, Remmert M, Soding J, Thompson JD, and Higgins DG (2011) Fast, scalable generation of high-quality protein multiple sequence alignments using Clustal Omega, Mol Syst Biol 7, 539. [PubMed: 21988835]

[44]. Schneider TD, and Stephens RM (1990) Sequence logos: a new way to display consensus sequences, Nucleic Acids Res 18, 6097–6100. [PubMed: 2172928]

[45]. Varadi M, Anyango S, Deshpande M, Nair S, Natassia C, Yordanova G, Yuan D, Stroe O, Wood G, Laydon A, Zidek A, Green T, Tunyasuvunakool K, Petersen S, Jumper J, Clancy E, Green R, Vora A, Lutfi M, Figurnov M, Cowie A, Hobbs N, Kohli P, Kleywegt G, Birney E, Hassabis D, and Velankar S (2022) AlphaFold Protein Structure Database: massively expanding the structural coverage of protein-sequence space with high-accuracy models, Nucleic Acids Res 50, D439–D444. [PubMed: 34791371]

[46]. Huynh K, and Partch CL (2015) Analysis of protein stability and ligand interactions by thermal shift assay, Curr Protoc Protein Sci 79, 28 29 21–28 29 14.

[47]. Kranz JK, and Schalk-Hihi C (2011) Protein thermal shifts to identify low molecular weight fragments, Methods Enzymol 493, 277–298. [PubMed: 21371595]

[48]. Cannon TM, Lagarto JL, Dyer BT, Garcia E, Kelly DJ, Peters NS, Lyon AR, French PMW, and Dunsby C (2021) Characterization of NADH fluorescence properties under one-photon excitation with respect to temperature, pH, and binding to lactate dehydrogenase, OSA Contin 4, 1610–1625. [PubMed: 34458690]

[49]. Gruber TD, Borrok MJ, Westler WM, Forest KT, and Kiessling LL (2009) Ligand binding and substrate discrimination by UDP-galactopyranose mutase, J Mol Biol 391, 327–340. [PubMed: 19500588]

[50]. Timson DJ (2006) The structural and molecular biology of type III galactosemia, IUBMB Life 58, 83–89. [PubMed: 16611573]

[51]. Shan M, Yang D, Dou H, and Zhang L (2019) Fucosylation in cancer biology and its clinical applications, Prog Mol Biol Transl Sci 162, 93–119. [PubMed: 30905466]

[52]. Miyoshi E, Moriwaki K, and Nakagawa T (2008) Biological function of fucosylation in cancer biology, J Biochem 143, 725–729. [PubMed: 18218651]

[53]. Wang W, Okajima T, and Takeuchi H (2022) Significant Roles of Notch O-Glycosylation in Cancer, Molecules 27, 1783. [PubMed: 35335147]

[54]. Ehmke N, Caliebe A, Koenig R, Kant SG, Stark Z, Cormier-Daire V, Wieczorek D, Gillessen-Kaesbach G, Hoff K, Kawalia A, Thiele H, Altmuller J, Fischer-Zirnsak B, Knaus A, Zhu N, Heinrich V, Huber C, Harabula I, Spielmann M, Horn D, Kornak U, Hecht J, Krawitz PM, Nurnberg P, Siebert R, Manzke H, and Mundlos S (2014) Homozygous and compound-heterozygous mutations in TGDS cause Catel-Manzke syndrome, Am J Hum Genet 95, 763–770. [PubMed: 25480037]

[55]. Schwarz FP, Puri K, and Surolia A (1991) Thermodynamics of the binding of galactopyranoside derivatives to the basic lectin from winged bean (Psophocarpus tetrogonolobus), J Biol Chem 266, 24344–24350. [PubMed: 1761537]

[56]. Brandts JF, Hu CQ, Lin LN, and Mos MT (1989) A simple model for proteins with interacting domains. Applications to scanning calorimetry data, Biochemistry 28, 8588–8596. [PubMed: 2690944]

[57]. Shrake A, and Ross PD (1988) Biphasic denaturation of human albumin due to ligand redistribution during unfolding, J Biol Chem 263, 15392–15399. [PubMed: 3170588]

[58]. Manly SP, Matthews KS, and Sturtevant JM (1985) Thermal denaturation of the core protein of lac repressor, Biochemistry 24, 3842–3846. [PubMed: 3902076]

[59]. Edge V, Allewell NM, and Sturtevant JM (1985) High-resolution differential scanning calorimetric analysis of the subunits of Escherichia coli aspartate transcarbamoylase, Biochemistry 24, 5899–5906. [PubMed: 3910085]

[60]. Sanchez-Ruiz JM, Lopez-Lacomba JL, Mateo PL, Vilanova M, Serra MA, and Aviles FX (1988) Analysis of the thermal unfolding of porcine procarboxypeptidase A and its functional pieces by differential scanning calorimetry, Eur J Biochem 176, 225–230. [PubMed: 3416871]

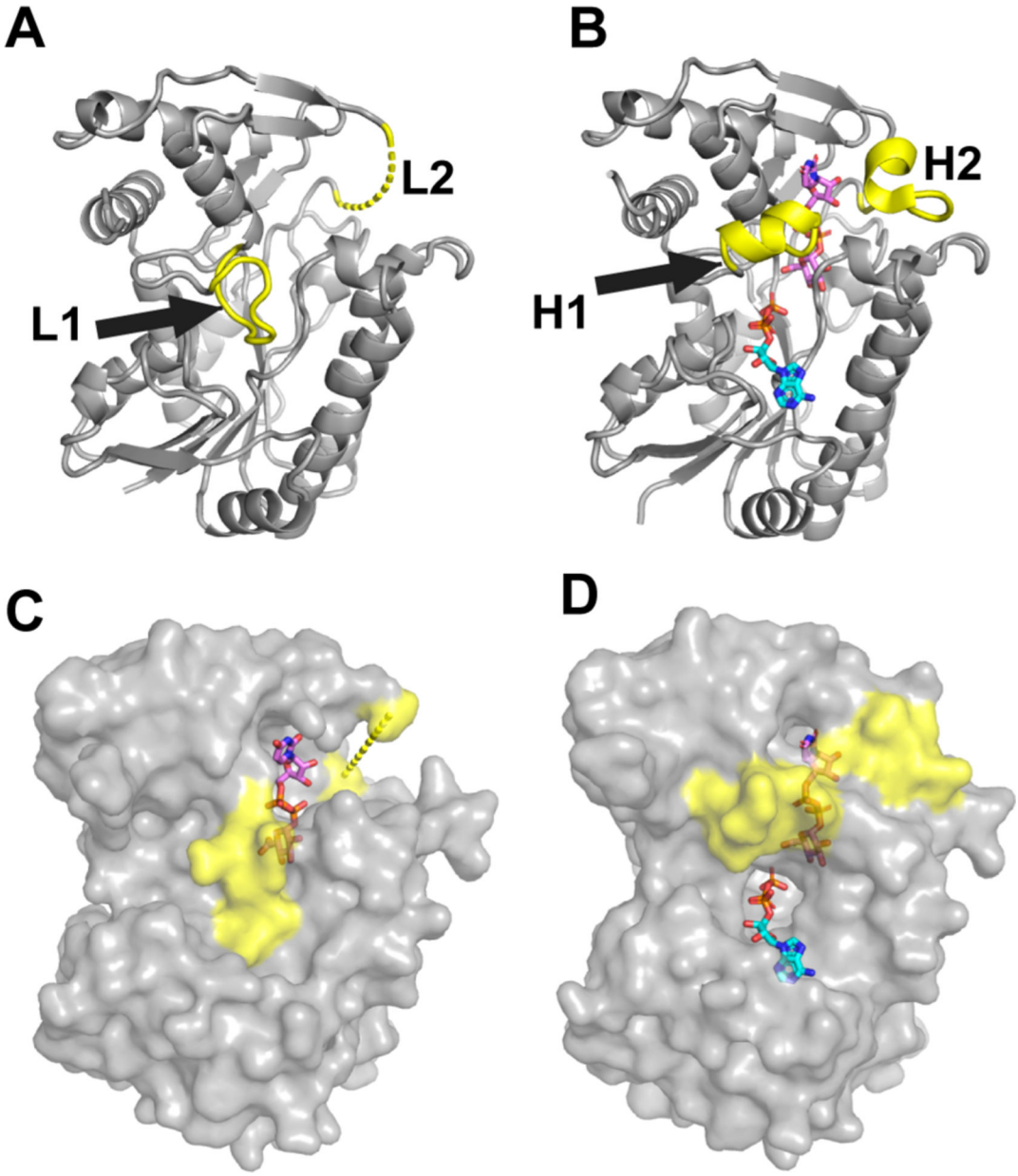

Figure 1.

The conformational change in *E. coli* ArnA dehydrogenase. Cartoon (A and B) and surface (C and D) representations of apo ecArnA_DH (A and C, PDB ID 1U9J) and ArnA_DH in complex with UDP-GlcA and ATP (B and D, PDB ID 1Z7E). Loops L1 and L2 in the apo structure and helices H1 and H2 in the liganded structure are highlighted in yellow; UDP-GlcA and ATP are shown as stick models in magenta and cyan respectively. In the surface representation of apo ArnA_DH (C), UDP-GlcA is shown modeled in its binding site for reference. The dotted lines denote unmodeled segments of the structure.

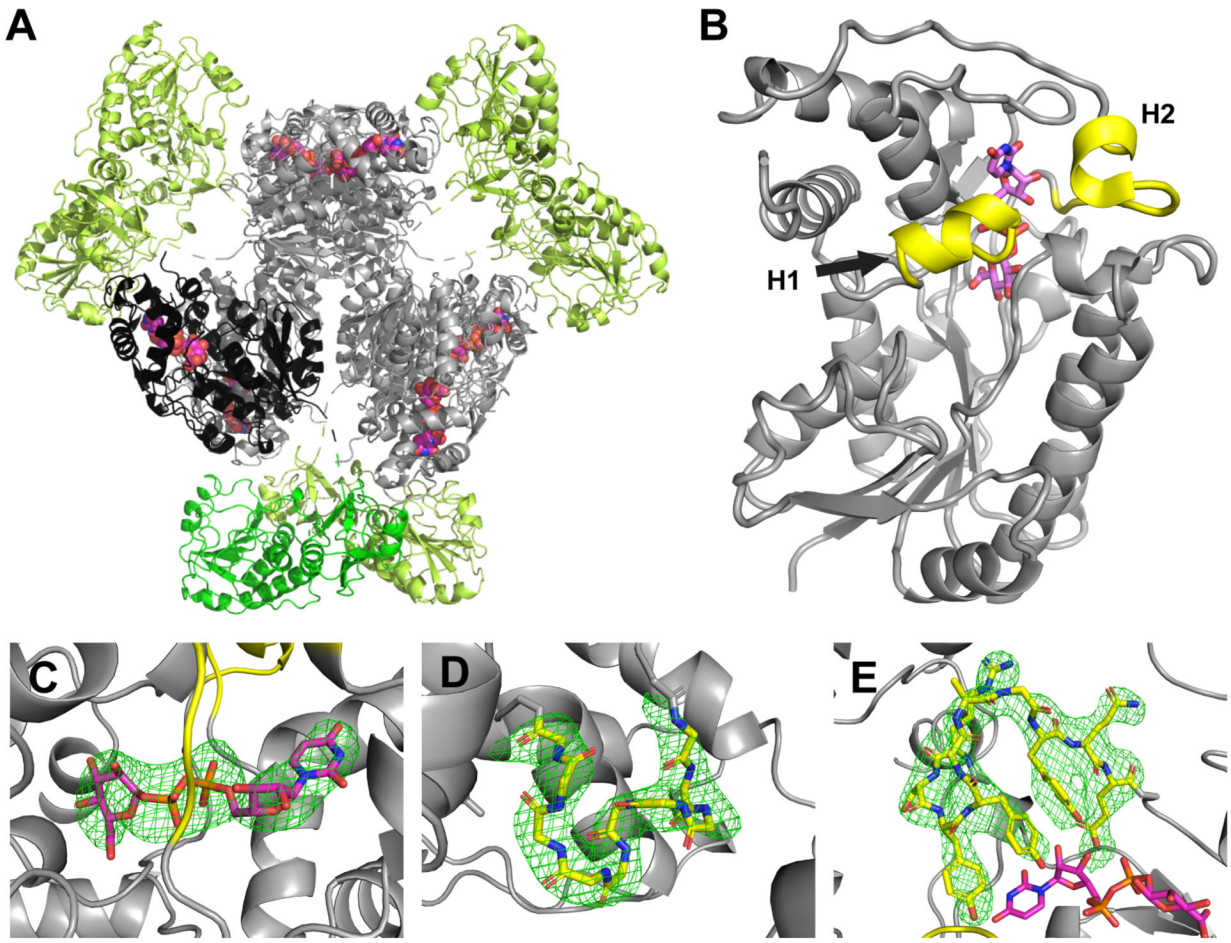

Figure 2.

Crystal structure of *Salmonella* Typhimurium ArnA. (A) Cartoon representation of the stArnA hexamer. The N-terminal transformylase domains are light green with monomer A shown in bright green; the C-terminal dehydrogenase domains are gray with monomer A shown in black. Bound UDP-GlcA is shown as space filling models with magenta carbons. (B) Dehydrogenase domain of stArnA. H1 and H2 helices are highlighted in yellow and the bound UDP-GlcA is shown as a stick model with magenta carbons. (C, D and E) Simulated annealing Fobs-Fc difference omit maps contoured at 3.0 sigma for the UDP-GlcA (C), the H1 helix (D) and the H2 helix (E). The ligand (C), H1 main chain atoms (D), and H2 atoms (E) in the refined models are shown as sticks superimposed with the electron density for reference.

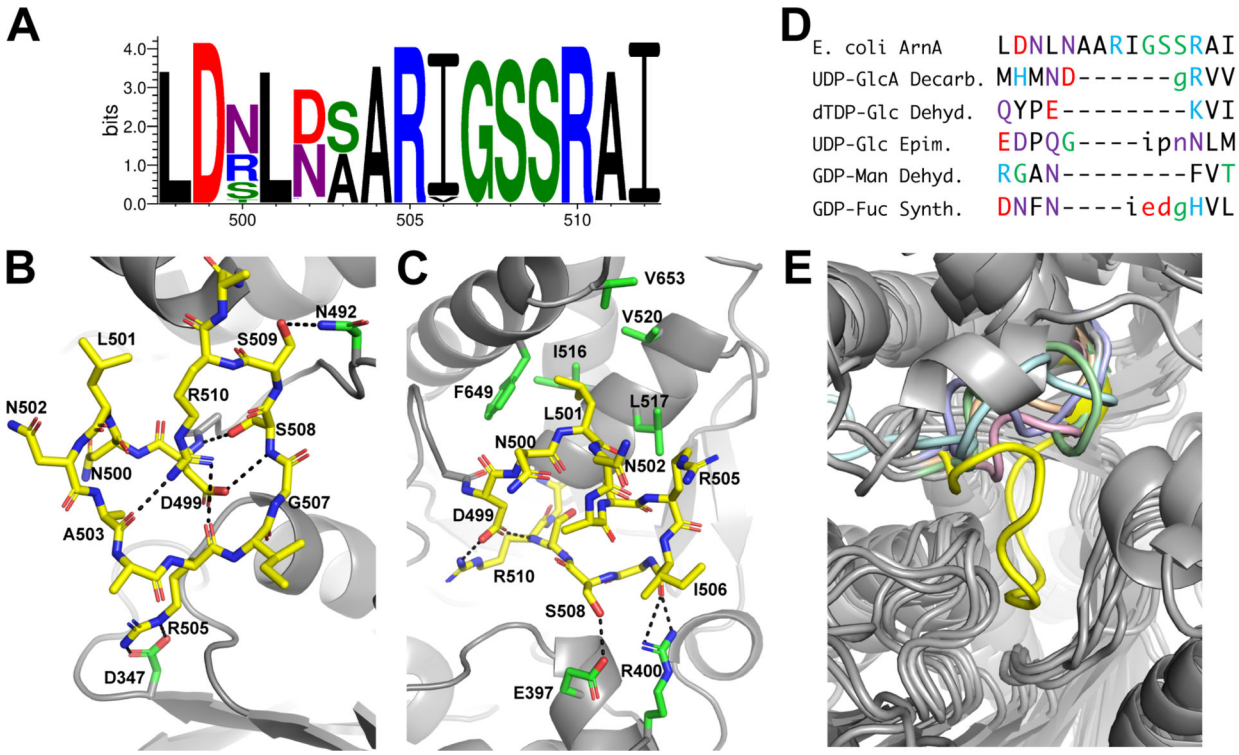

Figure 3.

The L1 loop in ArnA_DH orthologs and human homologs. (A) Logos representation of sequence conservation of residues 498–512 in ArnA_DH across diverse Gram-negative bacteria. (B and C) Stick representations of residues 500–510 of ecArnA_DH in the apo (B) and ligand bound (C) conformations. L1/H1 residues are shown in yellow, interacting residues in the rest of the protein are shown in green. (D) Structure-based sequence alignment of residues 498–512 in ecArnA_DH and its human homologs. Uppercase and lowercase letters represent superimposed and not-superimposed residues respectively. Dashes indicate gaps in the alignment. (E) Close up view of the L1 loop in ecArnA_DH superimposed to its human homologs. All proteins are colored gray except the L1 loop region of ecArnA_DH (yellow), UDP-GlcA decarboxylase (violet), dTDP-Glc 4,6-dehydratase (light orange), UDP-Glc epimerase (light blue), GDP-Man 4,6-dehydratase (light pink), and GDP-Fuc synthase (light green).

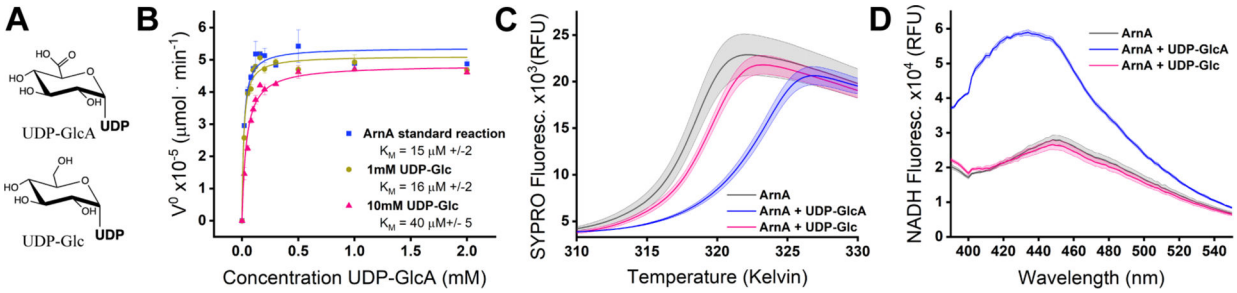

Figure 4:

UDP-glucose is a poor inhibitor of ArnA_DH and does not trigger the L1 to H1 conformational change. (A) Chemical structures of the sugar moieties in UDP-glucuronic acid (UDP-GlcA) and UDP-glucose (UDP-Glc). (B) Dehydrogenase activity of ArnA_DH in the absence of UDP-Glc (blue), or the presence of 1 mM (olive) or 10 mM (pink) UDP-Glc. Each reaction was performed in triplicate, with error bars representing the standard deviation. The lines are the best fit to a Michaelis-Menten hyperbola with the K_M values shown in the inset. (C) Thermal stability shift assay melting curves for ArnA_DH (black curve), ArnA_DH with 1 mM UDP-GlcA (blue curve), and ArnA_DH with 1 mM UDP-Glc (pink curve). (D) Conformational change assessed via NADH spectral changes upon binding. NADH fluorescence emission spectra were measured in a plate reader with 340 nm excitation in the presence of ArnA (black curve), ArnA and 1 mM UDP-GlcA (blue curve) or ArnA_DH and 1mM UDP-Glc (pink curve).

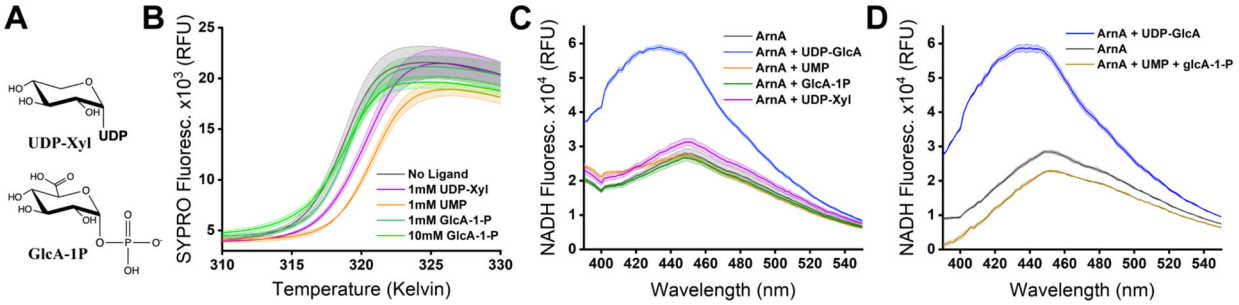

Figure 5:

UDP-GlcA analog binding and ability to trigger ArnA_DH conformational change. (A) Chemical structures of the sugar moieties in UDP-xylose (UDP-Xyl) and glucuronic acid-1-phosphate (GlcA-1P). (B) Thermal stability shift assay melting curves of ArnA_DH with no ligand (gray curve, T_m = 318.4 ± 0.03 K), 1 mM UDP-Xyl (purple curve, T_m = 320.0 ± 0.03 K), 1 mM UMP (orange curve, T_m = 320.6 ± 0.02 K), and 1 mM GlcA-1P (dark green curve, T_m = 318.9 ± 0.02 K) or 10 mM GlcA-1P (bright green curve, T_m = 318.4 ± 0.03 K). (C) Conformational change assessed via NADH spectral changes upon protein binding. NADH fluorescence emission spectra were measured in a plate reader with 340 nm excitation in the presence of ArnA_DH (black curve) or ArnA_DH and 1mM UDP-GlcA (blue curve), UDP-Xyl (purple curve), UMP (orange curve), or GlcA-1P (green curve). (D) Conformational change assay with UMP and GlcA-1P combined. The experiment is the same as in (C) for NADH in the presence of ArnA_DH (black curve) or ArnA_DH and 1mM UDP-GlcA (blue curve), or ArnA_DH and 10 mM UMP and 10 mM GlcA-1P (yellow curve). Background fluorescence from 10 mM UMP was subtracted from this curve.

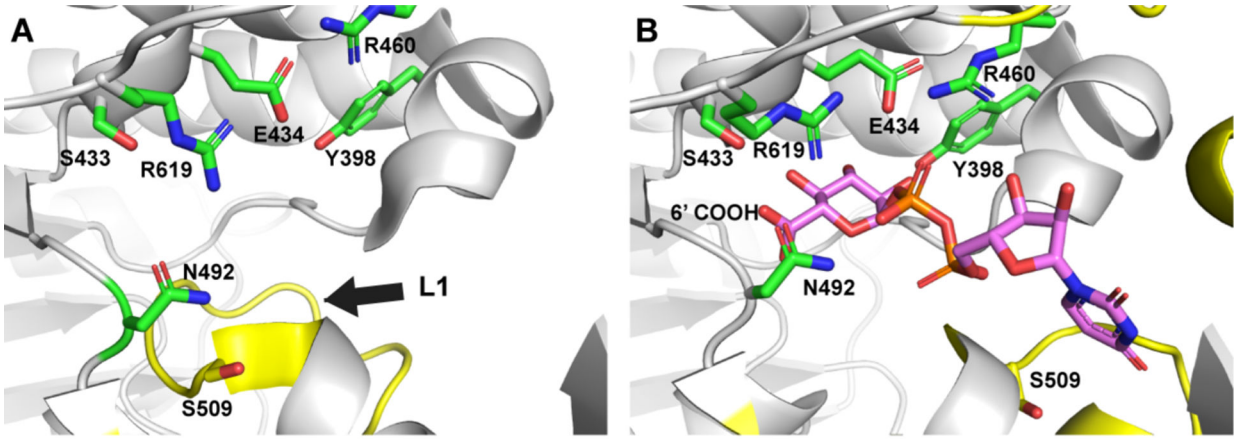

Figure 6:

UDP-GlcA binding site of ecArnA_DH in the apo (A) and ligand-bound (B) conformations. The L1 loop is highlighted in yellow and indicated by a black arrow in the apo structure. UDP-GlcA is shown as a stick representation in magenta with the 6' carboxylic acid labeled (6' COOH). The side chains of N492 and S509 are highlighted in green and yellow respectively. The side chains of selected residues that interact with UDP-GlcA are also shown in green. The segment for residues 528–538 is not shown for clarity.

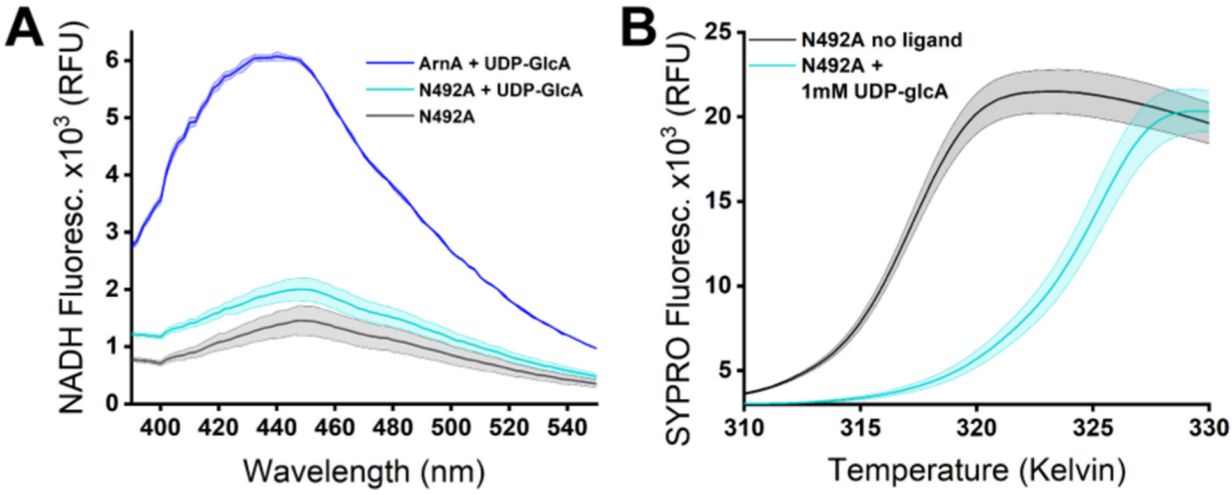

Figure 7:

Conformational change and ligand binding assays for ArnA_DH_N492A mutant. (A) Conformational change assessed by NADH spectral changes upon binding. NADH fluorescence emission spectra were measured in a plate reader with 340 nm excitation in the presence of ArnA_DH_N492A (black curve), ArnA_DH_N492A and 10 mM UDP-GlcA (cyan curve), or ArnA_DH wild type (WT) and 10 mM UDP-GlcA (blue curve). (B) Thermal stability shift assay melting curves for ArnA_DH_N492A in the absence (black curve) or presence (cyan curve) of 1 mM UDP-GlcA.

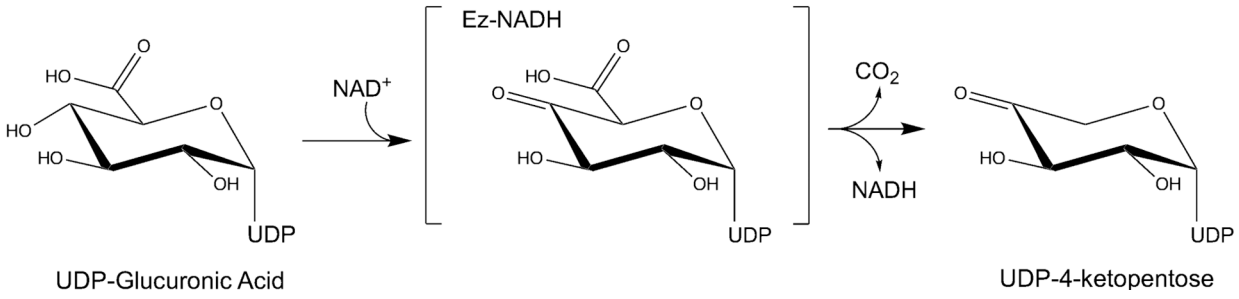

Scheme 1.
ArnA Dehydrogenase Catalyzed Reaction